Estimation of a semi parametric model of fMRI data

François G. Meyer
Department of Electrical Engineering, University of Colorado at Boulder
Department of Radiology, University of Colorado Health Sciences Center
E-mail: francois.meyer@colorado.edu.

ABSTRACT

This work provides a new approach to estimate the parameters of a semi-parametric generalized linear model in the wavelet domain. The method is illustrated with the problem of detecting significant changes in fMRI signals that are correlated to a stimulus time course. The fMRI signal is described as the sum of two effects : a smooth trend and the response to the stimulus. The trend belongs to a subspace spanned by large scale wavelets. We have developed a scale space regression that permits to carry out the regression in the wavelet domain while omitting the scales that are contaminated by the trend. Experiments with fMRI data demonstrate that our approach can infer and remove drifts that cannot be adequately represented with low degree polynomials. Our approach results in a noticeable improvement by reducing the false positive rate and increasing the true positive rate.

1. INTRODUCTION

In this paper we address the problem of estimating the parameters of a semi-parametric generalized linear model of a time series of the form :

$$y(t) = \theta(t) + \beta x(t) + \sigma^2 \nu(t) \tag{1}$$

where $\theta(t)$ is a smooth trend, $x(t)$ is a deterministic signal, β is a scalar that we are trying to estimate, and $\sigma^2 \nu(t)$ is a white noise process. This model allows to describe the fMRI response to a stimulus $x(t)$. The fMRI signal, $y(t)$, is contaminated by a random noise and a systematic baseline drift $\theta(t)$. Baseline drifts in fMRI data have been described by linear,[1,2] and polynomial[3,4] functions of time. The first contribution of this work is a new model of the drift that belongs to a subspace spanned by large scale wavelets. The second contribution of the work is a new method to estimate the drift $\boldsymbol{\theta}$ and to test for the significance of the response β to the stimulus. The method performs a scale space regression in the wavelet domain with the scales of the drift being omitted.

2. SOME WAVELETS NOTATIONS

We introduce in this section the notations associated with a discrete wavelet transform. These notations will be used in the sequel of the paper. Let $\Psi(t)$ be the wavelet, and let $\Phi(t)$ be the scaling function associated with a multiresolution analysis.[5] Let $\{h_n\}$ be the lowpass filter, and let $\{g_n\}$ be the high pass filter associated with this wavelet transform. Let $\mathbf{x} = \{x_n\}$, $n = 0, \cdots, N-1$ be a discrete signal. For the simplicity of the presentation we assume that $N = 2^J$. The wavelet coefficients of $\mathbf{x}$ are defined by the following recursions :

$$sx_k^0 = x_k \qquad k = 0, \cdots, N-1 \tag{2}$$

$$sx_k^{j+1} = \sum_n g_{n-2k}\, sx_n^j \;\; k = 0, \cdots, 2^{-j-1}N - 1 \tag{3}$$

$$dx_k^{j+1} = \sum_n h_{n-2k}\, sx_n^j \;\; k = 0, \cdots, 2^{-j-1}N - 1 \tag{4}$$

The wavelet transform $\mathbf{W}$ at scale J is a linear operator that maps $\mathbf{x}$ to $\mathbf{W}\mathbf{x}$ given by :

$$\begin{aligned}[sx_0^J, dx_0^J,\; dx_0^{J-1}, dx_1^{J-1}, \cdots, dx_0^j, \cdots dx_{2^{-j}N-1}^j,\\ \cdots\cdots\cdots, dx_0^1, \cdots\cdots, dx_{2^{-1}N-1}^1]^t.\end{aligned} \tag{5}$$

We also require that the wavelet ψ have p vanishing moments. As a consequence, polynomials of degree $p-1$ will have a very sparse representation in such a wavelet basis : all the d_k^j are equal to zero, except for the coefficients located at the border of the dyadic subdivision ($k = 0, 1, 2, 4, \cdots, 2^{J-1}$).

3. MODEL OF THE FMRI SIGNAL

Functional MRI can detect and quantify hemodynamic changes induced by brain activation and neuronal activity. Most of the current methods of analysis of fMRI data rely on an experimental paradigm consisting of ON (active) and OFF (rest) periodic stimulations of the subject. A commonly employed method to estimate the effect of the stimulus at a given voxel $\mathbf{M}$ in the brain relies on the linear model associated with the two sided Student's t-test, and assumes that the fMRI signal $\mathbf{y_M}$ at $\mathbf{M}$ is given by

$$y_{i,\mathbf{M}} = \beta_{\mathbf{M}}\, x_i + \sigma^2 \nu_{i,\mathbf{M}} \quad , \quad i = 0, \cdots, N-1 \tag{6}$$

where $\mathbf{x} = [x_0, \cdots, x_{N-1}]^t$ is the stimulus time course, composed of -1s (OFF) and 1s (ON). $\beta_{\mathbf{M}}$ is a scalar that measures the strength of the response to the stimulus induced by neuronal activation. $\beta_{\mathbf{M}}$ will be different from zero if the voxel $\mathbf{M}$ is inside a functionally activated brain area. $\boldsymbol{\nu}_{\mathbf{M}}$ =$[\nu_{0,\mathbf{M}}, \cdots, \nu_{N-1,\mathbf{M}}]^t$ is a white noise process caused by thermal and quantum noise.

Unfortunately, the detection of significant changes (measured by a significant $\beta_{\mathbf{M}}$) in the fMRI signal is further complicated by the presence of long term physiological drifts and instrumental instability that contribute to a systematic increase or decrease in the signal with time.[6,7] While the origin of the baseline drift is not completely understood,[2,7,8] it is obvious that if such baseline drifts are not removed, any analysis based on the model (6) will be tracking the large variation in the signal instead of the effects of the stimulus. In this work we propose to replace the model (6) with the following model :

$$y_{i,\mathbf{M}} = \theta_{i,\mathbf{M}} + \beta_{\mathbf{M}}\, x_i + \sigma^2 \nu_{i,\mathbf{M}}\ ,\ i = 0, \cdots, N-1 \tag{7}$$

where $\boldsymbol{\theta}_{\mathbf{M}} = [\theta_{0,\mathbf{M}}, \cdots, \theta_{N-1,\mathbf{M}}]^t$ is a baseline drift. In the sequel, we drop the $\mathbf{M}$ subscript to ease readability ; however, one should keep in mind that our method can effectively estimate a different trend for each voxel.

Our understanding of the origin of the drift[7] does not provide us with a specific function, or even a parametric model of the drift. Our assumption is that the trend is a superposition of physical and physiological phenomena that occur at different time scale, but that do not vary greatly over a short interval of time. An appropriate model for the trend is thus provided by a linear combination of large scale wavelets :

$$\theta(t) = s\theta_0^J \Phi(2^{-J}t) + \sum_{j=J_0}^{J} \sum_{k=0}^{2^{-j}N-1} d\theta_k^j \psi(2^{-j}t - k). \tag{8}$$

This model assumes that all the fine scale coefficients, $d\beta_k^j$, $1 \le j \le J_0 - 1$ of $\boldsymbol{\beta}$ are zero. The finest scale J_0 characterizes the complexity of the trend. Because the wavelet has p vanishing moments, the polynomials of degree $p-1$ will be approximated with a small error. This non parametric model of the trend not only describes the low frequencies fluctuations in the signal (encoded by the wavelet coefficients $s_k^J, d_k^J, ...$), but it also describes rapid localized changes, as is shown in Fig. 4. It is important to note that a model based on a Fourier expansion of the trend would miserably fail to describe localized changes, unless almost all of the harmonics were included in the model.

4. MAXIMUM LIKELIHOOD ESTIMATION

We describe here a method to estimate the vector $\boldsymbol{\theta}$, and the scalar β from a single time series $\mathbf{y}$. The estimation is done in the wavelet domain, and a Student's t-test can be performed on the wavelet coefficients to assess the significance of β. Applying the wavelet transform $\mathbf{W}$ on both sides of equation (7), yields :

$$\mathbf{W}\mathbf{y} = \mathbf{W}\boldsymbol{\theta} + \beta\mathbf{W}\mathbf{x} + \mathbf{W}\boldsymbol{\nu} \tag{9}$$

Because $\mathbf{W}$ is an orthonormal transform, $\mathbf{W}\boldsymbol{\nu}$ is a Gaussian white noise. Let $n_0 = 2^{-J_0+1}N$ be the number of coefficients that describe the trend. Our model of the trend is

$$\mathbf{W}\boldsymbol{\theta} = \left[s\theta_0^J, d\theta_0^J, \cdots, d\theta_{2^{-J_0}N-1}^{J_0}, 0, \cdots\cdots, 0 \right]. \tag{10}$$

Equation (9) can be written as a standard regression problem :

$$\mathbf{W}\mathbf{y} = \mathbf{A}\boldsymbol{\xi} + \mathbf{W}\boldsymbol{\nu} \tag{11}$$

where the $n \times (n_0 + 1)$ matrix $\mathbf{A}$ is given by :

$$\mathbf{A} = \begin{bmatrix} 1 & & & 0 & sx_0^J \\ & 1 & & 0 & dx_0^J \\ & & \diagdown & | & \vdots \\ & & & 1 \quad 0 & dx^{J_0}_{2^{-J_0}N-2} \\ & & & 1 & dx^{J_0}_{2^{-J_0}N-1} \\ & & & 0 & dx_0^{J_0-1} \\ & & & | & \vdots \\ & & & 0 & d^1_{2^{-1}N-1} \end{bmatrix} \tag{12}$$

and the $n_0 + 1$ vector $\boldsymbol{\xi}$ is

$$\boldsymbol{\xi} = \left[s\theta_0^J, d\theta_0^J, \cdots, d\theta^{J_0}_{2^{-J_0}N-1}, \beta \right] \tag{13}$$

The maximum likelihood estimate of $\boldsymbol{\xi}$ is given by :

$$\hat{\boldsymbol{\xi}} = [\mathbf{A}^t \mathbf{A}]^{-1} \mathbf{A}^t \mathbf{W} \mathbf{y} \tag{14}$$

Let $\mathcal{P}_{J_0}$ the projector onto the first $2^{-J_0+1}N$ coordinates

$$(\mathcal{P}_{J_0}\mathbf{x})_i = \begin{cases} x_i & \text{if} \quad i = 0, \cdots, 2^{-J_0+1}N - 1 \\ 0 & \text{otherwise} \end{cases} \tag{15}$$

and let $\mathcal{Q}_{J_0}$ be the projector onto the last $N - 2^{-J_0+1}N$ coordinates ($\mathcal{P}_{J_0} + \mathcal{Q}_{J_0} = \mathbf{I}$). It can be shown[9] that the maximum likelihood estimates are given by :

$$\hat{\beta} = \frac{< \mathcal{Q}_{J_0}\mathbf{W}\mathbf{x}, \mathcal{Q}_{J_0}\mathbf{W}\mathbf{y} >}{< \mathcal{Q}_{J_0}\mathbf{W}\mathbf{x}, \mathcal{Q}_{J_0}\mathbf{W}\mathbf{x} >} \tag{16}$$

and

$$\widehat{\boldsymbol{\theta}} = \mathbf{W}^{-1}\mathcal{P}_{J_0}(\mathbf{W}\mathbf{y} - \hat{\beta}\mathbf{W}\mathbf{x}) \tag{17}$$

This scale space regression permits to carry out the regression in the wavelet domain while omitting the scales that are contaminated by the trend. Because $\hat{\beta}$ is a Gaussian random variable, one can test its significance with a Student t-test with $N - n_0 - 1$ degrees of freedom.

5. MODEL SELECTION FOR THE TREND

The selection of the optimal value of J_0 is performed as follows. We start with $J_0 = J$ which provides the description of the trend with the minimum number of parameters. The significance of $\hat{\beta}$ is then tested, and we compute the P-value. We successively test more and more complex models of the trend by decreasing J_0. Because the scale of the trend should be larger than the scale of the stimulus, we stop before J_0 reaches the scale of the stimulus. Finally, one selects that J_0 which provides the smallest P-value. As shown in the experiments, the same value can be used for all activated voxels. This approach guarantees that the detrending algorithm will not increase the P values.

6. EXPERIMENTS

We illustrate here the principle of the algorithm with some data provided by Gregory McCarthy, (Brain Imaging and Analysis Center, Duke University), that demonstrate left posterior temporal lobe activation during auditory comprehension. [10] The study involved several subjects who listened passively to alternating sentences spoken in English (their native language), and Turkish (which they did not understand). Each time series was composed of 28 alternating auditory segments of English and Turkish. Each segment lasted for 6 seconds, and images were acquired every 1.5 s. There was a delay of 12 seconds from the first image to the onset of the first sentence. TR=1,500, slice thickness=9mm, skip = 2mm, imaging matrix= 128$\times$ 64, voxel size = 3.2 $\times$ 3.2 $\times$ 9 mm. More details about the experiments are available in. [10]

6.1. Effect of the detrending on the spectrum of the fMRI signal

A time series was extracted from the voxel (75,21) in slice 5, and is displayed in Figure 1. A discrete Fourier transform was computed (the signal was multiplied by a Gaussian window in order to enforce periodicity). The square of the Fourier coefficients are shown in Figure 2. As is obvious from Fig. 2 most of the energy lies at the low frequencies (note the logarithmic scale). Fig. 3 shows the spectrum of the detrended time series ($J_0 = 4$). The low frequencies have been removed, one can clearly detect the peak at the frequency of the stimulus (1/12 Hz).

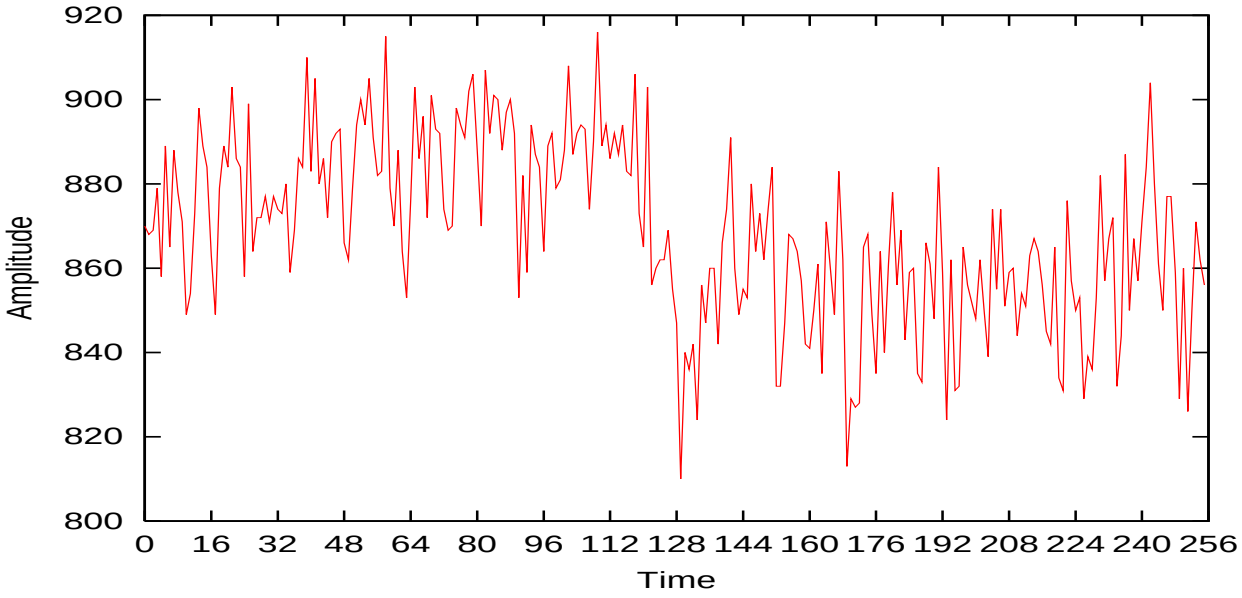

Figure 1. Time series of an activated voxel (75, 21, slice 4)

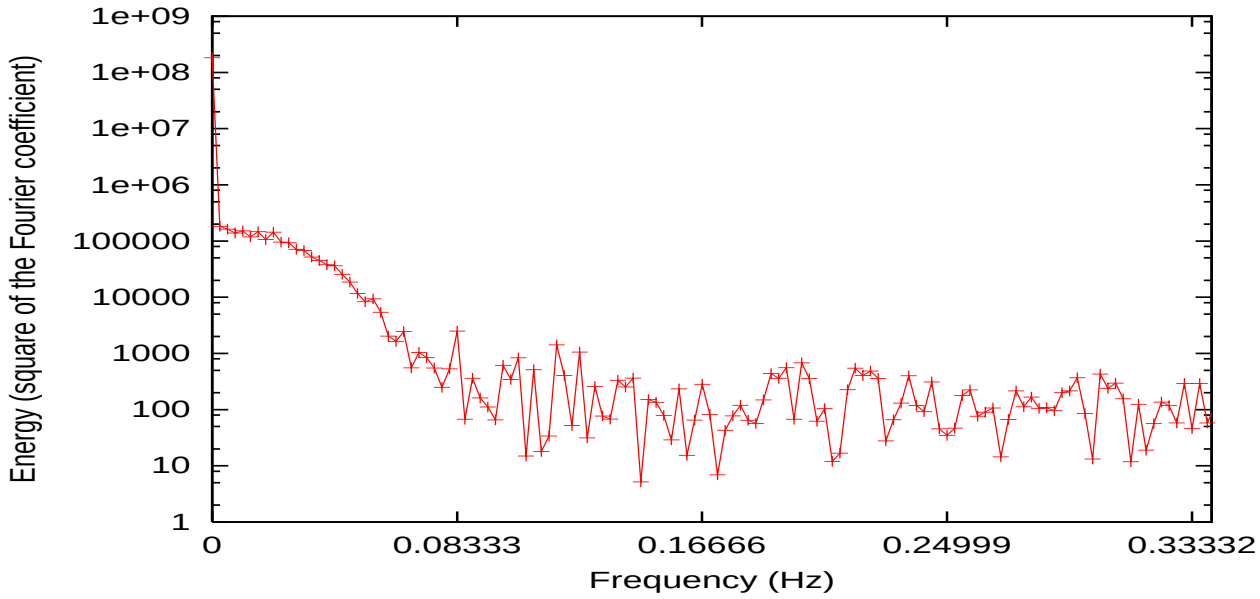

Figure 2. Power spectrum of the raw time-series. Most of the energy is located in the low frequency (note the logarithmic scale on the y axis).

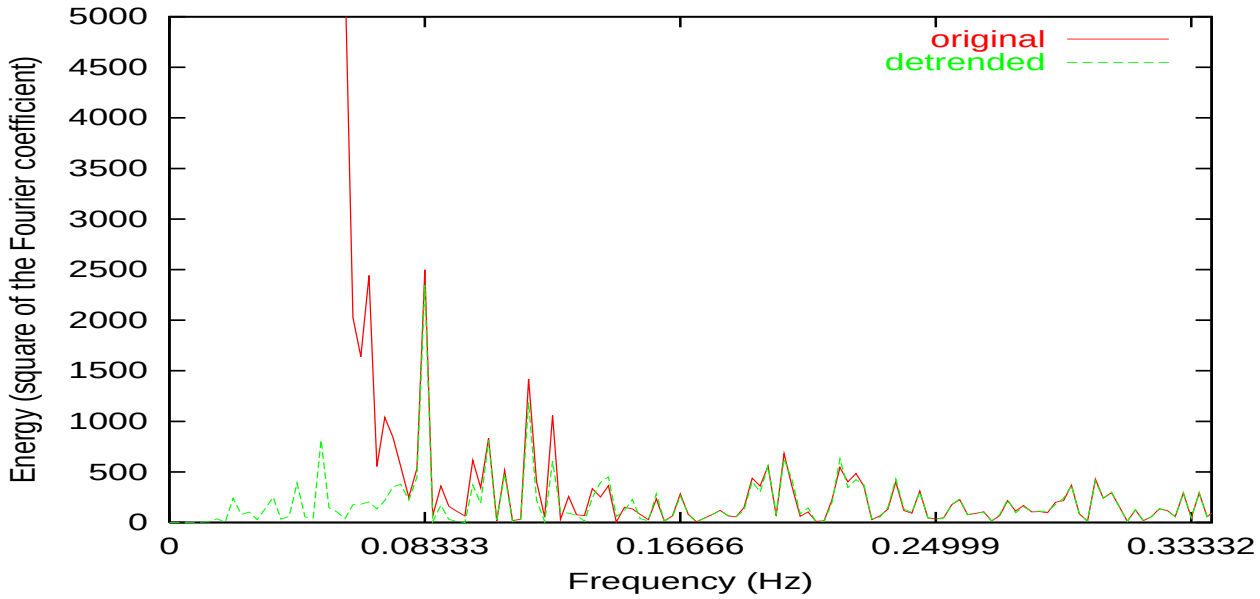

Figure 3. Power spectrum of the detrended time-series. The large scale (low frequencies) contaminants have been removed. The detrending has not removed the energy at the frequency of the stimulus (0.0833 Hz).

Figures 4,5,6 show the same time-series with the trend superimposed, for several values of J. We note that a piecewise linear trend (such as the one obtained for $J = 8$) fails to track the long term variability of the signal.

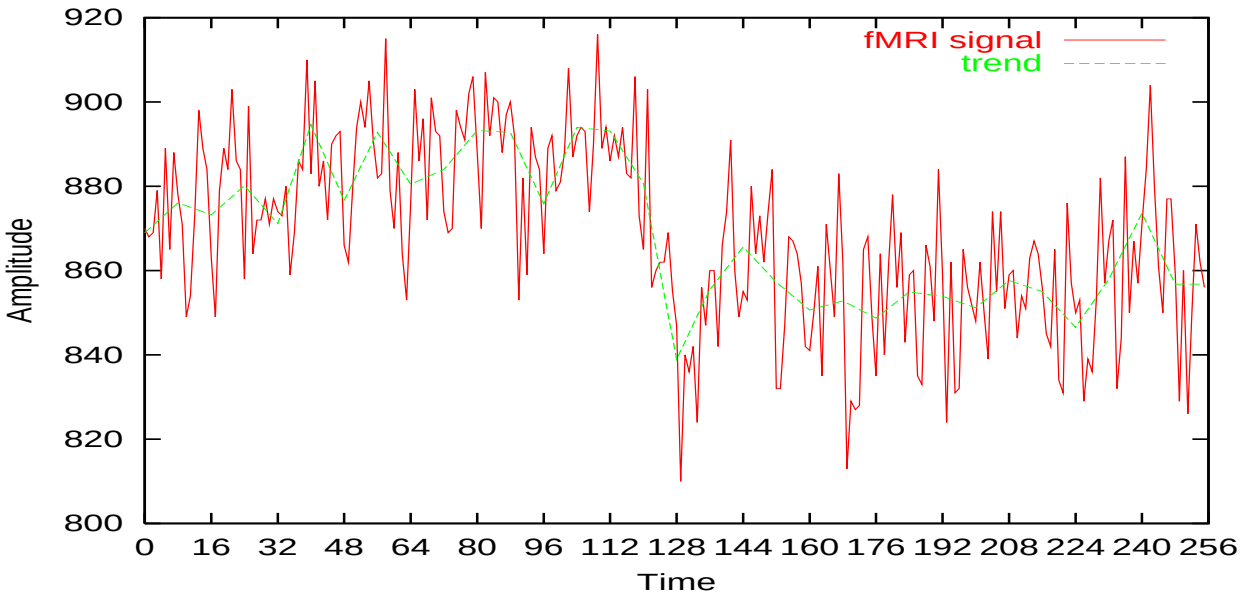

Figure 4. Trend for $J_0 = 4$.

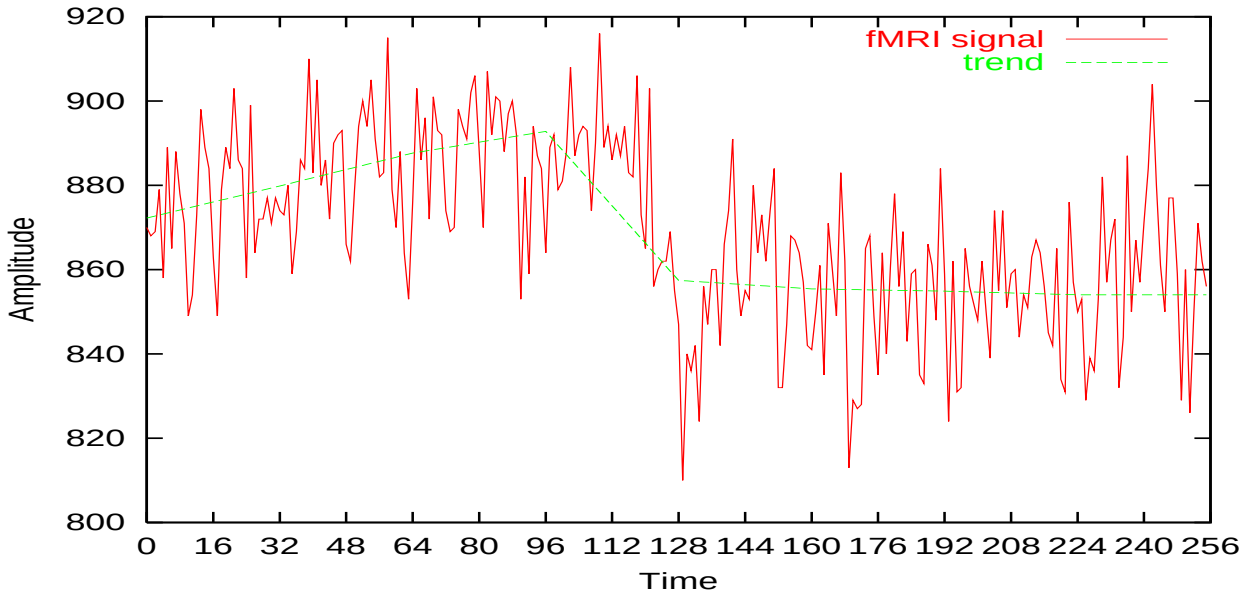

Figure 5. Trend for $J_0 = 6$.

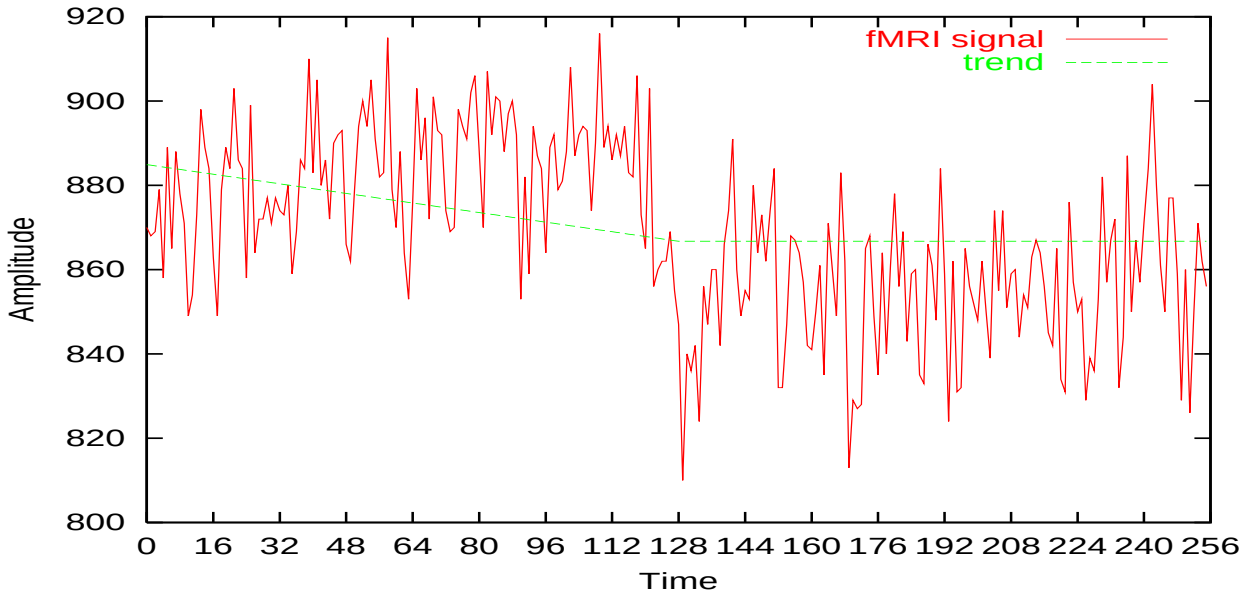

Figure 6. Trend for $J_0 = 8$.

6.2. Analysis of the detrending performance

We have compared the performance of the detrending algorithm for several values of the scale J_0 of the trend $\theta(t)$. The same value of J_0 was used for all pixels. We analyzed the performance of the detrending with two experiments using two different sets of data from the alternating English-Turkish experiment described in the previous section. A Student t-test was designed to compare the signal under the two conditions: English sentences, or Turkish sentences. Pixels with a P-value less than 0.005 were deemed activated, and colored in red in the activation maps.

6.2.1. Result of the first experiment

Figure 7 shows the result of the t-test for the slices 4 and 5 after detrending with $J_0 = 4$. The activation maps were thresholded at $P = 0.005$ and are superimposed on the raw EPI data. The left side of the brain is represented on the right side of the image. The maps were generated with two runs of alternating Turkish/English intervals, starting with Turkish. The maps clearly show activated pixels in the left inferior frontal lobe (region A and B).

For each slice we selected a region of interest (ROI) that contained strongly activated voxels ($P < 10^{-5}$). The activation in these regions was assumed to be truly caused by the stimulus and not by physiological or random noise. The two ROIs are shown as yellow rectangles, and are pointed at by the arrows A and B in slice 4 and 5 respectively. For each value of the scale of the trend, the performance of the detrending in each ROI was quantified using the following factors : (1) the number of activated voxels inside the ROI, (2) the mean P-value for all the voxels inside the ROI, and (3) the smallest P-value inside the ROI. These numbers are reported in tables 1 and 2. For both slices the detrending resulted in a noticeable improvement by increasing the number of activated voxels, while decreasing the mean P-value inside the ROIs. The optimal effect was obtained for a scale equal to 4. (The scale of the stimulus, as defined by the inverse of its frequency, was 2). One notes that as the scale of the trend becomes finer (e.g. $J_0 = 3$), the trend starts tracking the variations in the BOLD signal that are due to the stimulus response, and results in a poorer performance.

Because the ROIs in this experiment can be considered as truly activated voxels, this experiments demonstrates that the detrending helps to decrease the number of false positive. Indeed, on can significantly decrease the level of the threshold while keeping the truly activated voxel still activated in the ROIs A and B.

6.2.2. Result of the second experiment

A second experiment was conducted with a different data set. Figure 8 shows the result of the t-test for the slices 3 and 4 after detrending with $J_0 = 4$. The activation maps were thresholded at $P = 0.005$ and are superimposed on the raw EPI data. The maps were generated with two runs of alternating English/Turkish intervals, starting with English. The maps show in red activated pixels in the left posterior temporal lobe (regions C and D).

For each slice we again selected a region of interest (ROI) that contained strongly activated voxels ($P < 10^{-3}$). We note that the mean P-value before detrending was not as high as in the previous experiment. The two ROIs are shown as yellow rectangles, and are pointed at by the arrows A and B in slice 4 and 5 respectively. For each value of the scale of the trend, the performance of the detrending in each ROI was quantified using the same factors as in the previous experiments. These numbers are reported in tables 3 and 4. For both slices the detrending resulted in a noticeable improvement by increasing the number of activated voxels, while keeping the mean P-value inside the ROIs at the same value. The optimal effect was again obtained for a scale equal to 4.

This experiment demonstrates that detrending can help reducing the number of false negative : after detrending, there were 4 times more voxels activated in the ROI D, than before detrending.

7. CONCLUSION

In this paper we addressed the problem of estimating the parameters of the semi-parametric generalized linear model (7). This model allows to describe the fMRI response to a stimulus contaminated by a random noise and a systematic baseline drift. The trend belongs to a subspace spanned by large scale wavelets. We have developed a scale space regression that permits to carry out the regression in the wavelet domain while omitting the scales that are contaminated by the trend. Experiments with fMRI data demonstrate that our approach can infer and remove drifts that cannot be adequately represented with low degree polynomials. Our approach results in a noticeable improvement by reducing the false positive rate and increasing the true positive rate.

Acknowledgments

This work was supported by a Whitaker Foundation Biomedical Engineering Research Grant.

The author thanks Gregory McCarthy, Director of the Brain Imaging and Analysis Center, Duke University, for making the fMRI data available for this work.

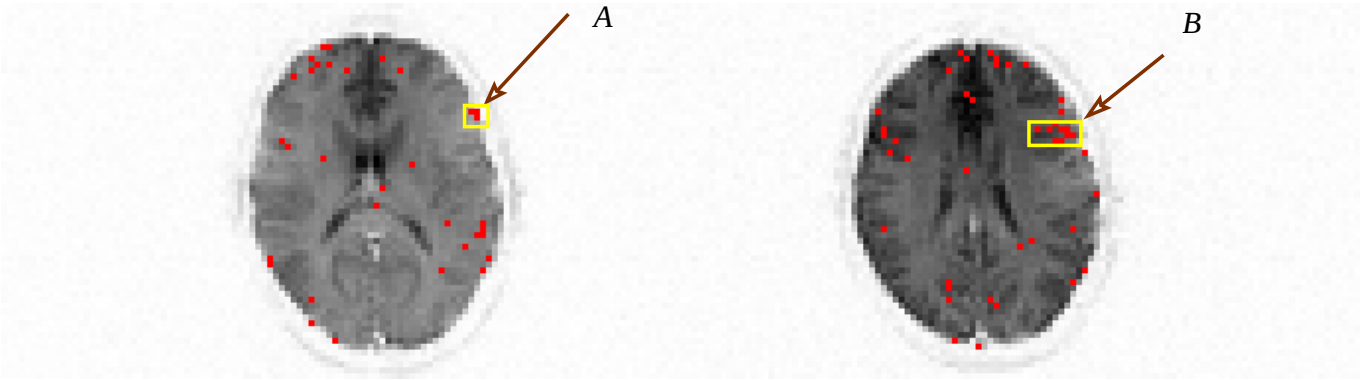

Figure 7. Turkish-English. Left : slice 4. Right : slice 5. Activation map thresholded at $p = 0.005$ superimposed on the raw EPI images. The scale of the trend was 4.

Scale of the trend: J_0	number of activated voxels	mean P-value	minimum of the P-values
3	1	6.9002e-05	6.9002e-05
4	3	1.3635e-05	4.5712e-06
5	3	1.5684e-04	8.1659e-06
6	3	1.8352e-04	8.0012e-06
7	3	7.2717e-04	1.0785e-05
8	2	6.4172e-05	6.069e-05
No trend	2	1.2959e-04	7.1008e-05

Table 1. Turkish-English, slice 4. Effect of the detrending inside the ROI A (4 voxels).

Scale of the trend: J_0	number of activated voxels	mean P-value	minimum of the P-values
3	3	2.207e-05	1.1775e-05
4	4	1.820e-04	3.3331e-08
5	4	2.477e-04	1.0355e-07
6	4	3.157e-04	2.0995e-07
7	4	3.434e-04	2.3841e-07
8	3	9.106e-04	5.0458e-07
No trend	2	1.200e-03	8.8839e-07

Table 2. Turkish-English, slice 5. Effect of the detrending inside the ROI B (6 voxels).

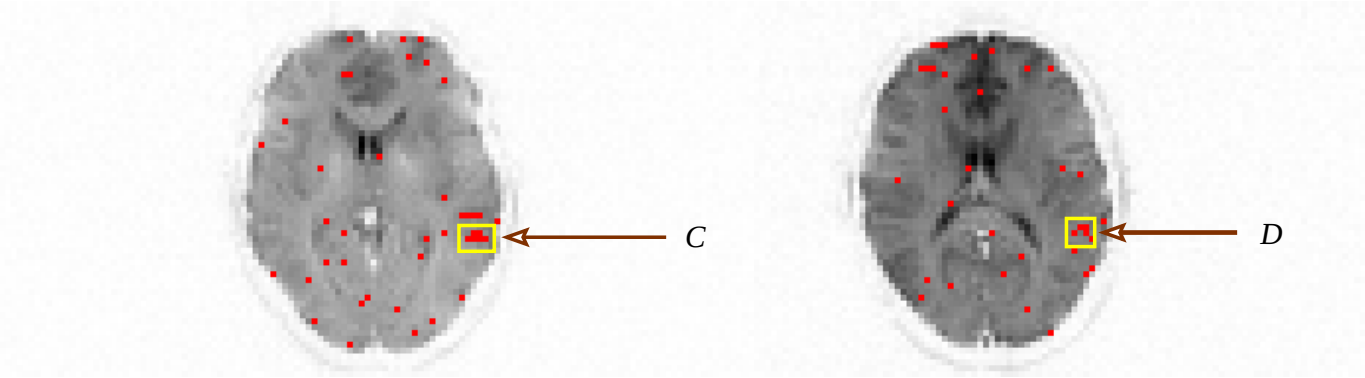

Figure 8. English-Turkish. Left : slice 3. Right : slice 4. Activation map thresholded at $p = 0.005$ superimposed on the raw EPI images. The scale of the trend was 4.

Scale of the trend: J_0	number of activated voxels	mean P-value	minimum of the P-values
3	4	2.1030e-03	8.6528e-05
4	6	1.1161e-03	4.2005e-06
5	5	8.1769e-04	1.3948e-05
6	6	1.8089e-03	1.8121e-05
7	5	1.3947e-03	3.2533e-05
8	5	1.3158e-03	6.3221e-05
No trend	4	1.2054e-03	3.7586e-04

Table 3. English-Turkish, slice 3. Effect of the detrending inside the ROI C (8 voxels).

Scale of the trend: J_0	number of activated voxels	mean P-value	minimum of the P-values
3	1	3.3086e-03	33086e-03
4	4	6.0944e-04	3.1159e-05
5	4	8.5158e-04	4.6997e-05
6	4	1.1497e-03	7.5901e-05
7	4	1.4909e-03	1.8074e-04
8	4	1.5032e-03	1.3863e-04
No trend	1	1.8923e-03	1.8923e-03

Table 4. English-Turkish, slice 4. Effect of the detrending inside the ROI D (9 voxels).

REFERENCES

1. P. Bandettini, A. Jesmanowicz, E. Wong, and J. Hyde, "Processing strategies for time-course data sets in functional MRI of the human brain," *Magn. Reson. Med.* **30**, pp. 161–173, 1993.
2. M. Lowe and D. Russell, "Treatment of baseline drifts in fMRI time series analysis," *Journal of Computer Assisted Tomography* **23(3)**, pp. 463–473, 1999.
3. G. Glover, "Deconvolution of impulse response in event-related bold fMRI," *NeuroImage* (9), pp. 416–429, 1999.
4. F. Kruggel, D. von Cramon, and X. Descombes, "Comparison of filtering methods for fMRI datasets," *NeuroImage* (10), pp. 530–543, 1999.
5. S. Mallat, *A Wavelet Tour of Signal Processing*, Academic Press, 1999.
6. P. Jezzard, "Physiological noise: strategies for correction," in *Functional MRI*, C. Moonen and P. Bandettini, eds., pp. 173–182, Springer-Verlag, 1999.
7. A. Smith, B. Lewis, U. Ruttimann, F. Ye, T. Sinnwell, Y. Yang, J. H. Duyn, and J. Frank, "Investigation of low frequency drift in fMRI signal," *NeuroImage* (9(5)), pp. 526–533, 1999.
8. V. Kiviniemi, J. Jauhiainen, O. Tervonen, E. Pääkkö, J. Oikarinen, V. Vainionpää, H. Rantala, and B. Biswal, "Slow vasomotor fluctuation in fMRI of anesthetized child brain," *Magn. Reson. Med.* **44**, pp. 373–378, 2000.
9. F. Meyer, "Wavelet based estimation of a semi parametric generalized linear model of fMRI time-series," tech. rep., Electrical Engineering, University of Colorado at Boulder, 2000.
10. M. Schlosser, N. Aoyagi, R. Fullbright, J. Gore, and G. McCarthy, "Functional MRI studies of auditory comprehension," *Human Brain Mapping* **6**, pp. 1–13, 1998.